Remote sensing of hydrocarbon layers by seabed logging (SBL): Results from a cruise offshore Angola

S. Ellingsrud, T. Eidesmo, and S. Johansen, ElectroMagnetic GeoServices, Trondheim, Norway
M.C. Sinha and L.M. MacGregor, School of Ocean and Earth Science, Southampton Oceanography Centre, Southampton, U.K.
S. Constable, Scripps Institution of Oceanography, La Jolla, California, U.S.

Detecting and assessing hydrocarbon reservoirs without the need to drill test wells is of major importance to the petroleum industry. Seismic methods have traditionally been used in this context, but the results can be ambiguous. Another approach is to use electromagnetic sounding methods that exploit the resistivity differences between a reservoir containing highly resistive hydrocarbons and one saturated with conductive saline fluids. Modeling presented by Eidesmo et al. (2002) demonstrates that by using seabed logging (SBL), a special application of frequency domain controlled source electromagnetic (CSEM) sounding, the existence or otherwise of hydrocarbon bearing layers can be determined and their lateral extent and boundaries can be quantified. Such information provides valuable complementary constraints on reservoir geometry and characteristics obtained by seismic surveying.

In November 2000, a full-scale trial survey was carried out from the research ship *RRS Charles Darwin* offshore Angola, in an area with proven hydrocarbon reserves. The project was a collaboration among Statoil, Scripps Institution of Oceanography, and the Southampton Oceanography Centre. The object was to demonstrate that SBL, developed by Statoil (Eidesmo et al., 2000; Ellingsrud et al., 2001), could direct detect hydrocarbon-filled layers in the subseafloor.

The petroleum prospects offshore Angola are in a deep Tertiary basin consisting of a thick (10-20 km) sequence of prograding sands and shales. The area is characterized by allochthonous salt of Aptian age, and deepwater channel sands with petroleum potential. Well logs show sediment resistivities typically around 0.7 Ωm that rise to around 100 Ωm in petroleum reservoirs. The survey site was on the continental slope in water depths of about 1200 m, with a known petroleum reservoir about 1100 m below seafloor. Shallow salt occurs in the northeast corner of the area.

Experimental method. The marine CSEM method employed in this survey uses a horizontal electric dipole (HED) source to transmit a discrete frequency electromagnetic signal from the source to an array of seafloor receivers. These receivers detect and record two orthogonal components of the horizontal electric field at the seafloor. The variation in the amplitude and phase of the received signal as the source is towed through the array of receivers can be used to determine subseafloor resistivity structure at scales that range from a few tens of meters to several kilometers. The method has been used in academia for many years, primarily to study ocean basins and active spreading centers. However, this survey is the first application to direct hydrocarbon detection.

The source was the DASI (deep-towed active source instrument) electromagnetic transmitter provided by the Southampton Oceanography Centre. This consists of a 100-m, neutrally buoyant, HED transmitter that streamed behind a deep-towed vehicle 40-50 m above the seafloor. The streaming height was chosen to be less than an electromagnetic skin depth in seawater to ensure good coupling of the transmitted signal into the seafloor, while simultaneously being far enough from the seabed to avoid collision with seafloor installations in the area. The source transmitted a pseudosquare waveform with a peak-to-peak amplitude of typically 305 A to give a source dipole moment of 16 500 Am at the fundamental transmission frequency. The source position was determined in real time using ultrashort baseline acoustic navigation between the ship and a transponder mounted on the front of the deep-tow vehicle. The ship was navigated using differential GPS.

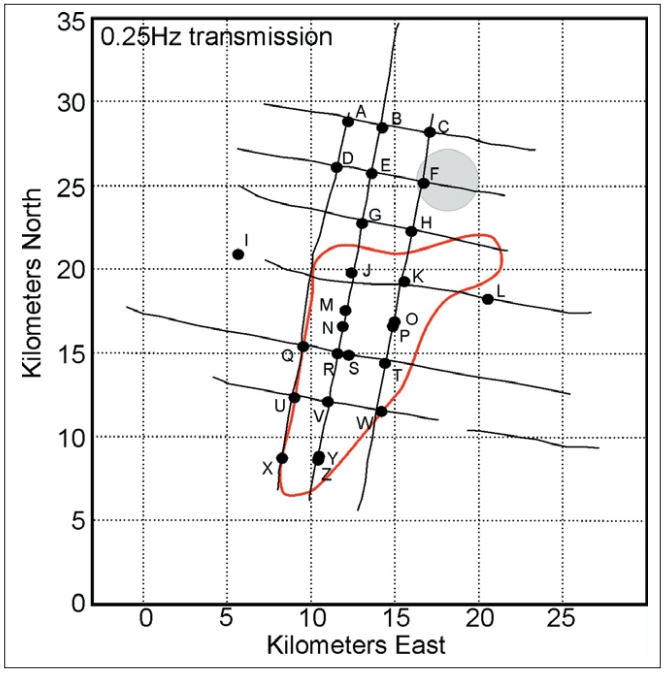

Figure 1. *Survey geometry for the 0.25-Hz and 0.75-Hz transmissions—26 receivers were deployed (filled circles) and the source was then towed through the array along towlines totaling 314 km (solid black lines). Receivers at sites C and H (both ELF instruments) were lost and those at I and P, although recovered, failed to record usable data. Also shown are the approximate outline of the known hydrocarbon reservoir (solid red line) and the position/approximate extent of the shallow salt body (grey circle).*

Twenty-six seafloor receivers were deployed for the survey. Twenty were supplied by Scripps—10 ELF receivers and 10 broadband magnetotelluric (MT) receivers. The remaining six instruments, LEMUR receivers, were supplied by Southampton Oceanography Centre and the University of Lisbon. All instruments detect and record two orthogonal components of the horizontal electric field at the seafloor by means of two receiver dipoles (lengths of 10 m and 13.5

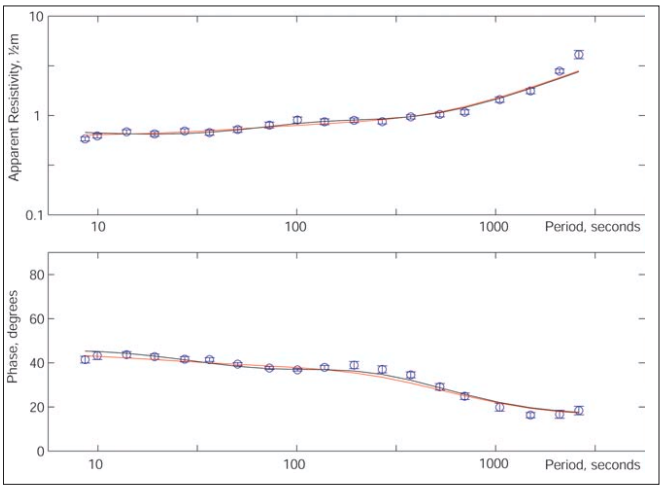

Figure 2. *Stacked response from 6 MT data sets, interpreted to be the TE mode, along with 1D model responses from the structures in Figure 3. Error bars were generated from the variance in the mean at each frequency and reflect the highly consistent nature of the original data sets. The red line corresponds to the maximally smooth model and the black line to a model with steps in resistivity at 2 and 15 km. Both models fit the data to rms 1.5.*

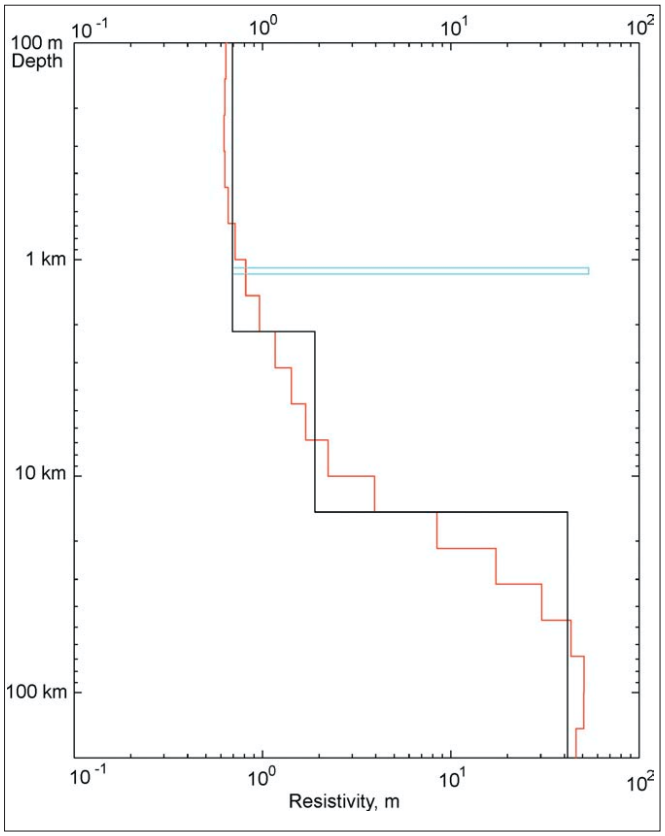

Figure 3. *1D model inversions of the MT data in Figure 2. Both the smooth model (red) and the layered model (black) fit the MT data to rms 1.5. The CSEM data are normalized by a simple model, consisting of the upper two layers of the layered MT model (black). The blue layer, invisible to MT sounding and representing the known depth and thickness of hydrocarbons, is needed to satisfy the radial CSEM data.*

m, respectively, for the ELF/MT and LEMUR receivers). Each receiver dipole is formed by two low-noise silver-silver chloride electrodes supported at the ends of plastic arms. The MT instruments also record two horizontal components of the seafloor magnetic field using induction coils mounted on the instrument frame. In addition to CSEM sounding, data from these instruments can be used for seafloor magnetotelluric sounding studies.

The target was chosen on the basis of the known geology in the area, forward modeling, and previous experience of instrumental performance. The survey geometry was then designed to optimize the sensitivity of the resulting data to the structures of interest. The design was for a primary survey conducted at a transmission frequency of 0.25 Hz, followed by a second survey at 1 Hz along a subset of the towlines. For each case, the receiver array and towlines were arranged to maximize geometric coverage. Figure 1 shows survey geometry for the 0.25 Hz transmission. Over the eight days of the survey, the source was towed along 17 lines with a total length of 314 km, to give 110 hours of CSEM data on each receiver. Of the 26 instruments deployed, 23 were recovered at the end of the cruise, and another was recovered subsequently with an ROV. All but two of those recovered (one LEMUR and one MT) recorded data.

A vertical mooring with four current meters at 20 m intervals 10-70 m above the seafloor was deployed near the center of the survey area (in water depth of 1320 m) at the start of operations. It remained in place until CSEM operations were completed. Each meter measured water temperature, conductivity, speed, and current direction at two-minute intervals. Throughout the survey, the conductivity of the near-bottom seawater was 3.36-3.42 S/m, and the temperature was 4.00-4.15° C. During the first part of the survey, water currents were generally less than 10 cm/s in a northerly direction. In the second half of the survey, current speed increased to 25-30 cm/s in a southeasterly direction.

Magnetotelluric data. The object of collecting MT data during this survey was to provide an independent estimate of the background conductivity profile. Because the MT method is blind to the presence of thin resistive layers, the conductivity structure obtained using MT is ideal for normalizing the CSEM data (Eidesmo et al., 2002). In addition, MT data can be used to exclude an increase in resistivity at depth that could mimic the effect of thin resistors in the radial fields (Eidesmo et al., 2002).

The MT instruments were deployed at the beginning of the survey so that data could be collected for several days before the EM transmitter started to operate. Because the EM receivers saturate at source-receiver ranges less than about 1 km, MT data cannot be processed during transmission, even though the CSEM signal is only a narrow-band noise source. Sites B, E, L, M, N, T, V, and Z were processed simultaneously using the multistation algorithm of Egbert (1997). Only V failed to produced clean, consistent MT responses between 8 and 3000 s, although the response from L at periods longer than 1000 s had higher apparent resistivities/lower phases and may have been biased by coherent noise. Data were essentially one dimensional at periods shorter than 100 s and weakly 2D at longer periods with a principal axis of 150°W, which corresponds approximately to the downdip slope of the bathymetry. When rotated, the xy resistivities all varied randomly about an average sounding curve, and varied by no more than a factor of 1.5 (excluding site L). The yx resistivities, however, varied systematically, by a factor of 3, from resistive in the north to conductive in the south. We thus interpret the xy curves to be the TE mode (electric fields parallel to strike) and the most appropriate for 1D interpretation. We averaged TE data from the six best sites to produce a composite curve, and estimated error bars from variance in the mean at each frequency. Figure 2 shows the resulting MT response.

The MT response was inverted using the OCCAM algorithm of Constable et al. (1987), which produces a maximally

smooth model for a given data misfit. It is possible to fit the data to rms 1.0, but the resulting oscillatory model clearly overfits the data. We chose a misfit of rms 1.5 to be suitably conservative. In the resulting model (Figure 3), we see a surface resistivity of 0.6-0.7 Ωm, in good agreement with well logs, increasing to several tens of Ωm at depth. The resistivity of the section could indeed increase steadily with depth, but most likely is made up of discrete lithological boundaries. If we relax the misfit penalty at depths of 2 and 15 km, we get a three-layer model that fits the data as well as before but with no gradients in resistivity (Figure 3). Figure 2 shows fits to these two models to the data. The depth of the first interface can be moved up or down somewhat, but the uppermost 1500 m of the section is constrained to be uniform and about 0.7 Ωm. Depth to electrical basement, at 15 km, agrees fairly well with the expected thickness of the sedimentary section in this area.

CSEM data processing. The raw CSEM data were continuous, unstacked time series of electric fields, recorded at a sample rate of 32 Hz for the ELFs, 25 and 31.25 Hz for the MT instruments, and 128 Hz for the LEMURs. Initial processing of ELF and LEMUR data involved taking Fast Fourier transforms (FFT) of data segments to extract the amplitude and phase of the signal at the fundamental transmission frequencies, 0.25 Hz and 1 Hz, and their third and fifth harmonics (0.75 Hz, 1.25 Hz, 3 Hz, and 5 Hz). Because the source waveform is a pseudosquare wave, amplitudes of the even harmonics are small. For the ELF and LEMUR instruments, these frequencies lie directly on Fourier bins so there is no sidelobe leakage. The FFT method thus provides an efficient way to carry out least squares fitting of the sinusoidal components of transmission. For the MT instruments, transmission frequencies do not fall exactly on Fourier bins for a data window 2^n samples in length; so an overdetermined least squares fit of sinusoids to data segments was carried out using QR decomposition to give results statistically equivalent to an FFT.

For the 0.25 Hz transmission, a data segment length of 256 s (for the ELF and LEMUR instruments) and 240 s (for the MT) instruments was used. However, because of drift in the time base of the source, these windows proved too long to process the higher frequencies, as phase shifting during the data window was sufficient to cause signal cancellation. The data were therefore reprocessed using 64-s (for the ELF and LEMUR instruments) and 60-s (for the MT instruments) data segments to extract the higher frequencies. Phase data at all frequencies was corrected to account for source phase drift. Finally, data were corrected for the frequency response of the instruments and normalized by the source dipole moment for ease of comparison with modeling results, which assume a unit dipole source.

Ambient noise levels on the instruments were estimated by applying the same processing procedures to data segments recorded prior to the start of DASI transmissions. Noise floors on most instruments were between 10^{-13} and 10^{-15} V/Am^2, with the MT instruments consistently quieter than the ELF or LEMUR instruments. All instruments exhibit noise between 0.1 and 0.01 Hz that appears correlated with the magnitude of water currents recorded by the current meter array. On some instruments, particularly in shallower water, the noise extended to the higher frequencies used in the CSEM survey, slightly degrading the noise floor during the latter half of the survey. The noise floors compare favorably with noise levels encountered on previous CSEM experiments.

Until the orientation of the seafloor instruments can be verified by careful inspection of the field components, it is appropriate to represent the CSEM data using the semimajor and semiminor axes of the polarization ellipse (Smith and Ward, 1974). The semimajor axis of the polarization ellipse provides a robust measure of the seafloor electric field because it is independent of the receiver orientation and less sensitive to errors in the source-receiver geometry than either electric field component separately. As a result, it formed the basis for preliminary interpretation of the data.

Preliminary 1D modeling. A simple and useful starting point in interpreting the data is to model subsets in terms of 1D layered earth structures. Modeling has demonstrated that, even for simple 1D structures, the response measured at the seafloor depends on the source-receiver geometry (MacGregor et al., 1998; MacGregor & Sinha, 2000; Eidesmo et al., 2002). Electric fields propagating along the axis of the source dipole (at a source-receiver azimuth of 0° or 180°—the in-line or radial geometry) interact with the subseafloor resistivity structure very differently from fields propagating perpendicular to the source dipole axis (at an azimuth of 90° or 270°—the broadside or azimuthal geometry). This difference, which can lead to a characteristic "splitting" of radial and azimuthal responses in the presence of hydrocarbon layers, is critical in resolving ambiguities in the interpretation of SBL data sets (Ellingsrud et al., 2002).

We will illustrate this via a data subset with radial fields recorded during the central north-south trending source tow and azimuthal fields (defined as those with an azimuth within plus or minus 5° of 90° or 270°) recorded during the six east-west trending tows by the receivers sited along the central north-south line. The central portion of this profile was over the reservoir target area (Figure 4). For clarity, only the radial fields from instruments M, V, and Y (see Figure 1) that lie over the reservoir, are shown. These instruments are all MT receivers, and therefore have a lower noise floor and higher data quality than the other instruments along the line. Note that data density for the azimuthal fields is much smaller than for the radial fields because radial data can be collected continuously during transmitter tow toward and away from a receiver, but azimuthal data can only be obtained from discrete crossing lines.

Wireline logging of wells in the area suggests that resistivity of overburden sediments is around 0.6 Ωm. The MT model agrees with the logs, but also shows that resistivity increases to about 2 Ωm at depth (the deeper electrical basement is far too deep to be detected by the CSEM survey). Our reference model is thus chosen to be a 0.6 Ωm layer, 2000 m thick and underlain by a 2 Ωm half space, in water depths of 1200 m (the average water depth in the survey area).

The dashed lines in Figure 4a show the radial and azimuthal responses of the reference model. It is clear that this background response, especially in the radial geometry, does not fit the data. Figure 4a also shows radial and azimuthal responses from an earth model consisting of a 75-m thick layer of 50 Ωm resistivity buried 1100 m below the seafloor. Using a resistivity structure comprising a 30-m thick 50 Ωm resistive layer, a 20m thick 1 Ωm shale layer followed by a 30-m thick 100 Ωm layer buried at 1100m depth, representing the true structure of the hydrocarbon reservoir makes only a small difference to the response. The response of the hydrocarbon model fits the data far better, correctly reproducing the trends in both the radial and azimuthal data.

In order to highlight the effect of the hydrocarbon layer, Figure 4b shows the data and response of the hydrocarbon

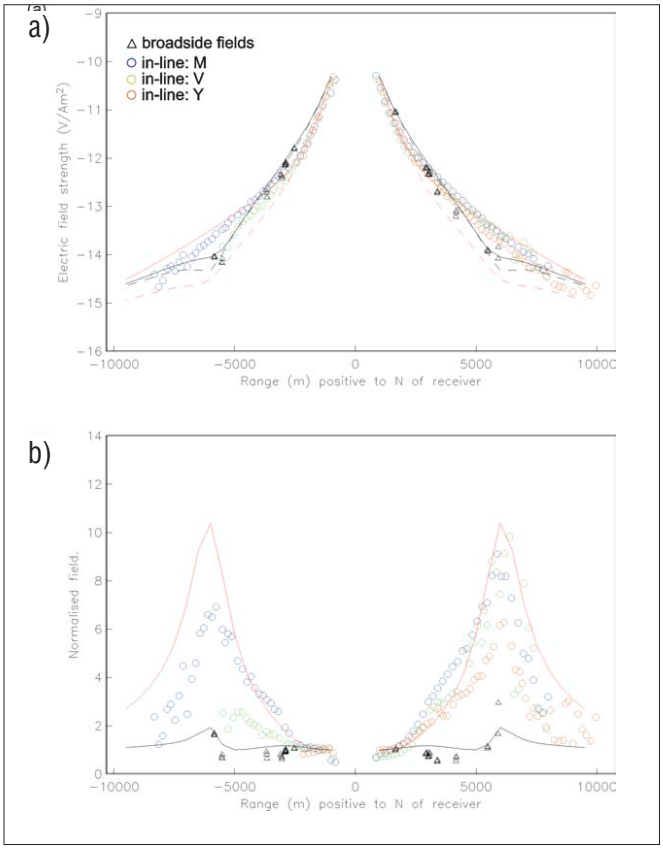

Figure 4. *(a) Radial and azimuthal geometry data from the center of the survey, plotted as a function of source-receiver separation (positive when the source is north of the receiver). Transmission frequency was 0.25 Hz. Radial data (circles) consist of data recorded by receivers M, V, and Y during the central north-south trending towline. Azimuthal data (triangles) consist of data at source-receiver azimuths within 5° of 90° and 270°, recorded by the receivers sited along this line, during the six east-west trending source tows. Red and black dashed lines show the radial and azimuthal (respectively) responses of the reference model described in the text. It is clear that this does not explain the data. Solid red and black lines are responses obtained by including a thin resistive (hydrocarbon) layer in the reference model (see Figure 3). They fit the data much better. (b) Data in (a) normalized by the reference model, in order to highlight the effect of the hydrocarbon layer. Also shown are normalized radial and azimuthal responses (red and black lines, respectively) of the 1D model that includes the hydrocarbon layer. The data closely follow the predicted model response.*

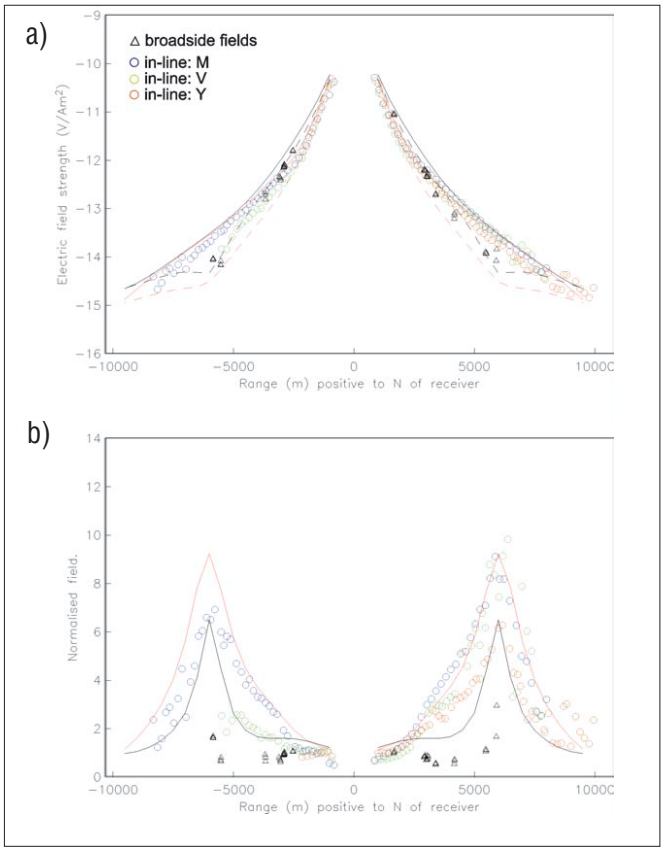

Figure 5. *(a) Radial and azimuthal geometry data from the center of the survey as in Figure 4, but compared to the radial and azimuthal responses (red and black lines respectively) of a 1D model in which resistivity increases steadily with depth (200 m thick, 0.5 Ωm layer over a 200 m thick, 1 Ωm layer, both overlying a 2 Ωm half space). For comparison, the red and black dashed lines show the radial and azimuthal (respectively) responses of the reference model. Although the model with increasing resistivity correctly predicts the radial data, it does not fit the azimuthal data. (b) Data and 1D model response shown in (a) normalized by the response of the reference model. Other parameters as in Figure 4b. Although the behavior of the radial response is correctly predicted by the increasing resistivity model, the "split" between the radial and azimuthal fields is not reproduced.*

model normalized by the response of the reference model. This demonstrates that the hydrocarbon model does fit the data, and in particular illustrates the "split" between radial and azimuthal geometries, which is characteristic of a hydrocarbon layer (Eidesmo et al., 2002; Ellingsrud et al., 2002).

Although this simple 1D model predicts the major trends in the data, it does not explain all details. Further 2D and 3D modeling (that takes into account the finite lateral extent of the hydrocarbon reservoir) will be necessary to fully explain all the features observed. However, Figure 4b suggests that the enhancement of the radial fields caused by the resistive hydrocarbon layer falls off for source positions south of receiver V, implying that the southern boundary of the hydrocarbon reservoir lies in this area.

For cases when exploration wells have been drilled in the survey area and the overburden resistivity is known, the enhancement of the radial fields can be used as an indicator of buried hydrocarbon layers. However, in most exploration situations, when the resistivity structure of the overburden is not known, care must be exercised in interpreting the data. This is illustrated in Figure 5, which shows the data from the center of the survey as in Figure 4, but this time compared to a 1D model without a hydrocarbon layer but in which overburden resistivity increases steadily with depth. Figure 5b shows that, although such a model can correctly predict the magnitude of the radial electric fields, the azimuthal response has a much larger magnitude than observed in the data. The steadily increasing resistivity model is probably not realistic for sediment basins—resistivity depends on porosity, pore sizes, tortuosity, formation water salinity, pressure and temperature—see discussion in Eidesmo et al., 2002; but it shows that only by collecting both radial and azimuthal data can the potential ambiguity between models containing thin resistive (potentially hydrocarbon bearing) layers be distinguished from other earth models. The collection of coincident MT data provides a good independent estimate of the background resistivity structure and would help avoid an erroneous interpretation.

Pseudoimaging. Although Figure 4 shows that the hydrocarbon-bearing reservoir beneath the survey area can be detected by the SBL data as collected, it uses only a small subset of the data and is based on a simple 1D model of the area. A second approach, which allows the data to be more readily visualized, is shown in Figures 6 and 7. Here the

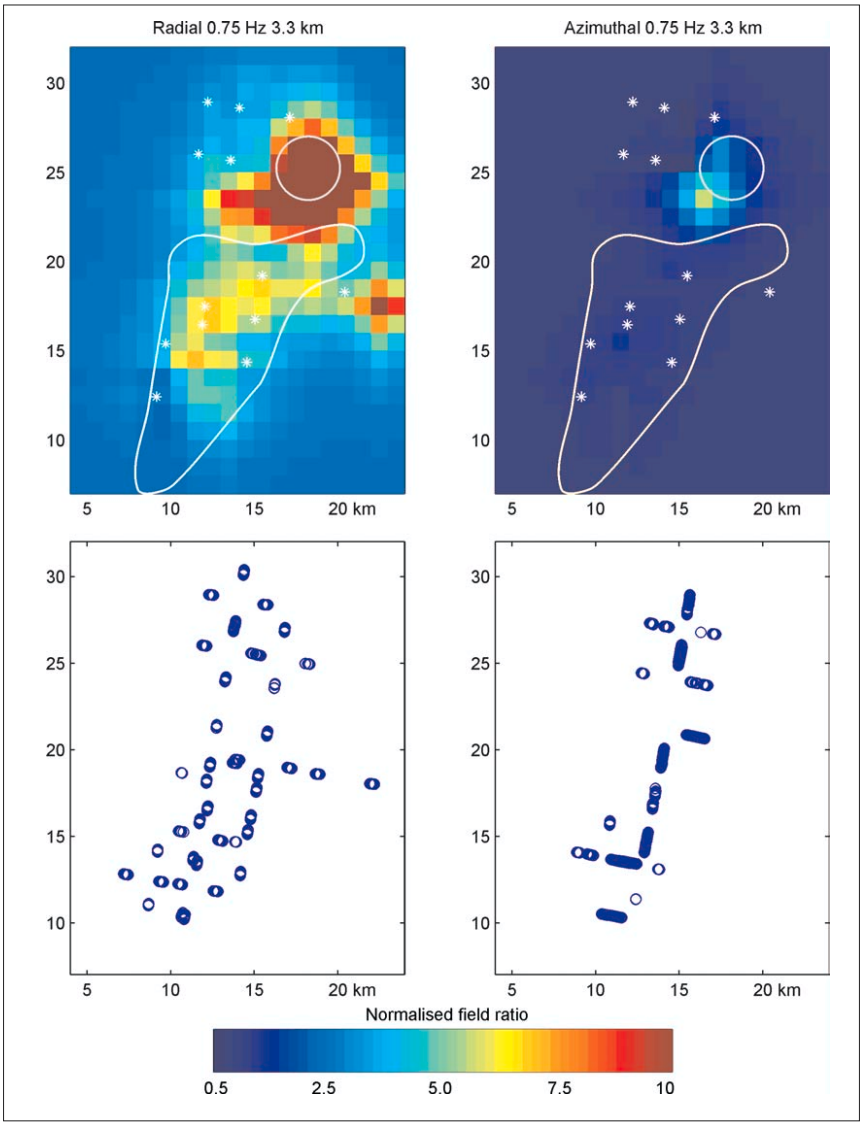

Figure 6. *Normalized magnitude of 0.75 Hz electric fields at the seafloor for a range bin of 3000-3600 m, plotted as a function of source-receiver midpoint across the survey area. Plotted for reference is the approximate outline of the known hydrocarbon reservoir (solid white line). Upper panels show the data and instrument locations used to generate the data, and the lower panels show the distribution of source-receiver midpoints used to generate the plots. Left panels show predominantly radial fields; right panels show predominantly azimuthal fields. The large anomaly in the northeast, visible in both radial and azimuthal fields, is a known salt body. The smaller anomalies which are confined to the radial data over the rest of the survey correspond to the known petroleum reservoir. Data to the south and northwest lack a significant radial response and show the limits on the lateral extent of the reservoir.*

fields (normalized by the reference model) have been sorted into source-receiver range bins, and the predominantly radial and azimuthal fields plotted as a function of source-receiver midpoint. This approach is much more qualitative than 1D modeling but it does allow a larger data set to be represented by a set of maps, providing an image that gives a rough indication of the spatial extent of the target response. Again, we have restricted our analysis to the best quality data sets, those from the MT instruments at sites B, E, L, M, N, T, V, and Z and ELFs at F, K, O, S, and U.

The left panels in Figure 6 show the normalized 0.75-Hz radial electric fields at the seafloor, for a source-receiver range of 3.3 km, along with the positions of the instruments and the source-receiver midpoints. The latter represent the density of the data set being contoured. The most obvious feature is the enhancement of fields in the northeast quadrant of the area, over the known location of salt. The salt is also represented in the azimuthal data (right panels), although the sparse data distribution of the azimuthal data results in a weaker anomaly. However, this demonstrates that the presence of a thick salt body affects both the radial and azimuthal fields. Figure 7 shows a similar data set for a frequency of 0.25 Hz and a range of 5 km. Again, salt dominates the radial field plot but is absent from the azimuthal field plot because there are no midpoints over the structure.

The reservoir is evident as enhanced radial fields in the south-central portion of our array at both 0.75 and 0.25 Hz. Although we have adequate azimuthal coverage in this area, there are no anomalous fields in the azimuthal data. As expected, the thin resistive reservoir layer produces enhanced radial fields while the azimuthal fields are only marginally altered. The southern boundary of the reservoir is fairly well determined by the radial fields, and it can be seen that data collected in the northern part of the survey west of the salt are also off the reservoir structure. The agreement between the region of enhanced radial fields and extent of the reservoir determined from drilling and seismic data analysis is good.

Discussion and conclusions. Both approaches above (1D forward modeling and pseudoimaging) provide clear indications that the normalized radial electric fields measured in the survey are substantially larger than the normalized azimuthal fields, leading to an amplitude split which is larger than can be generated by reasonable variations in the overburden resistivity. Simple 1D forward modeling at 0.25 Hz demonstrates that the measured fields agree well with the predicted electromagnetic response of the known hydrocarbon reservoir in the area. Our study was complicated by the fact that salt structure in the northeast part of the area enhances the electric fields. This, on the other hand, highlights the fact that electromagnetic surveying maps resistors, not hydrocarbons. However, adequate data from other sources, such as seismic and gravity, sufficiently rich CSEM geometries which include azimuthal as well as radial fields, and independent electrical data from MT sounding, all serve to protect the user from being caught by misinterpretation.

Our survey represents the first field-scale trial of the SBL method in the context of direct detection of hydrocarbons. Although preliminary, these results clearly indicate that this special application of the CSEM method has detected the hydrocarbon-bearing reservoirs beneath the seafloor. Full analysis of this data set will require further, more detailed, modeling analysis and interpretation, using higher dimensional approaches than the simple 1D modeling presented here. But our result paves the way for further SBL surveys to provide valuable complementary information to that gathered in more conventional methods of reservoir detection and characterization.

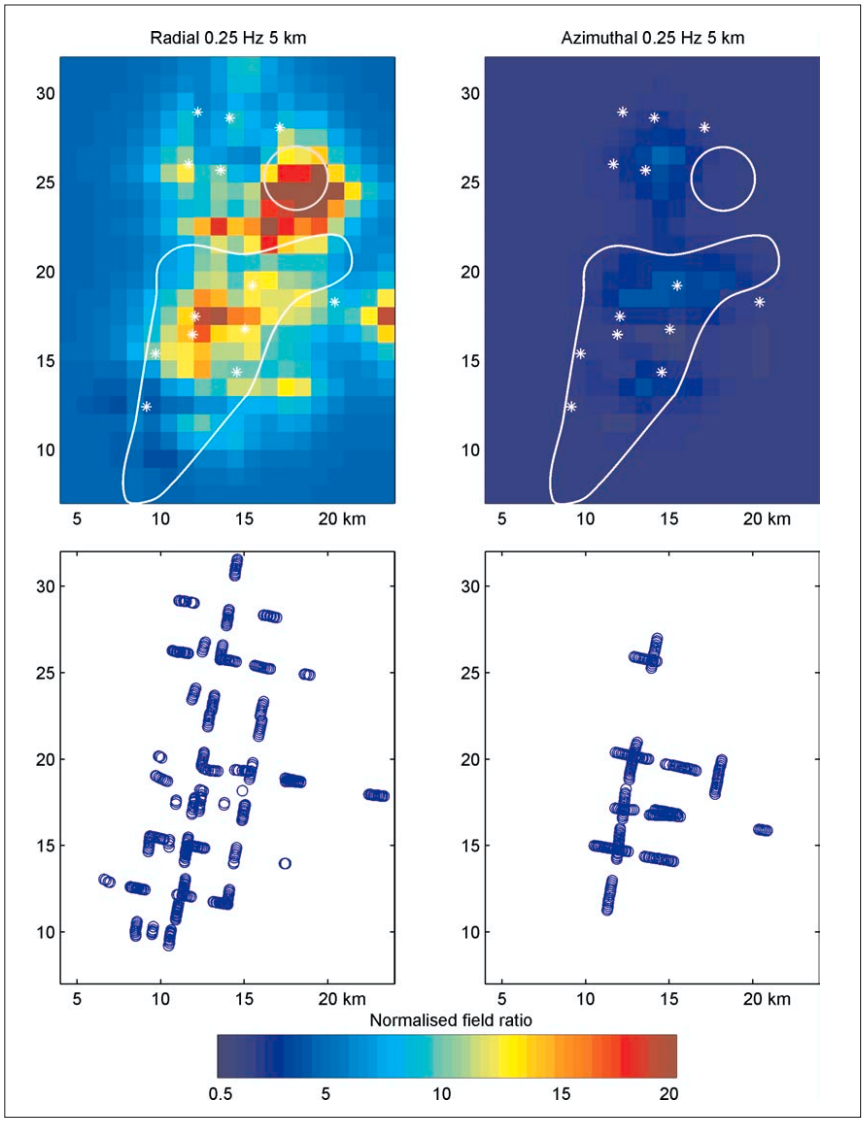

Figure 7. *Similar to Figure 6, but at 0.25 Hz and a range bin of 4000-6000 m.*

Suggested reading. "Marine controlled source electromagnetic sounding, II : The PEGASUS experiment" by Constable and Cox (*Journal of Geophysical Research*, 1996). "Marine magnetotellurics for petroleum exploration, Part I: A seafloor equipment system" by Constable et al. (GEOPHYSICS, 1998). "Occam's inversion: a practical algorithm for generating smooth models from EM sounding data" by Constable et al. (GEOPHYSICS, 1987). "Robust multiple station magnetotelluric data processing" by Egbert (*Geophysical Journal International*, 1997). "Seabed logging (SBL), a new method for remote and direct identification of hydrocarbon filled layers in deepwater areas" by Eidessmo et al. (*First Break*, 2000). "On the electrical nature of the axial melt zone at 13°N on the East Pacific Rise" by Evans et al. (*Journal of Geophysical Research*, 1994). "The RAMESSES experiment, III: Controlled source electromagnetic sounding of the Reykjanes Ridge at 57°45'N" by MacGregor et al. (*Geophysical Journal International*, 1998). "Electrical resistivity structure of the Valu Fa Ridge, Lau basin, from marine controlled source electromagnetic sounding" by MacGregor et al. (*Geophysical Journal International*, 2001). "An active source electromagnetic sounding system for marine use" by Sinha et al. (*Marine Geophysical Research*, 1990). "Short note on the computation of polarisation ellipse parameters" by Smith and Ward (GEOPHYSICS, 1974). "Electromagnetic active source sounding near the East Pacific Rise" by Young and Cox (*Geophysical Research Letters*, 1981). "Method and apparatus for determining the nature of subterranean reservoirs" by Eidesmo et al. (patent application WO 00/13046, 2000, filed August 1998). "Reservoir identification using refracted wave" by Ellingsrud et al. (patent application WO 01/57555, 2001, filed February 2000). "Method for electric dipole configuration on the seabed" by Ellingsrud et al. (International patent application (PCT) GB01/03473, priority date 14 August 2000. TLE

Acknowledgments: The authors thank the captain and crew of the R.R.S. Charles Darwin *and the staff of the Ocean Engineering Division of Southampton Oceanography Centre (SOC) for support of the marine operations. James Behrens and Kerry Key of Scripps Institution of Oceanography (SIO), Lisl Lewis of AOA Geophysics, and Antonio Soares of University of Lisbon provided invaluable help on board ship. Instrument development and preparation by Jennifer Rust of SOC and Jacques Lemire of SIO was critical to the success of the project. Salary support for LMM came from a NERC Research Fellowship. Support for instrumentation and salaries at SIO were provided in part by the Seafloor Electromagnetic Methods Consortium. Finally, the authors thank Angolan authorities for giving us the opportunity to test the SBL technique in their territorial waters and Sonangol for permission to publish these data.*

Corresponding author: sve@emgs.no